Supplementary Information

Photocatalysts Based on Cobalt-chelating Conjugated Polymers for Hydrogen Evolution from Water

Lianwei Li,[1] Ryan G. Hadt,[2] Shiyu Yao,[2] Wai−Yip Lo,[1] Zhengxu Cai,[1] Qinghe Wu,[1] Bill Pandit,[3] Lin X. Chen[2,3*] and Luping Yu[1*]

[1]Department of Chemistry and the James Franck Institute, The University of Chicago, 929 E 57th Street, Chicago, IL 60637, USA.

[2]Chemical Sciences and Engineering Division, Argonne National Laboratory, 9700 S Cass Avenue, Lemont, IL 60439, USA.

[3]Department of Chemistry, Northwestern University, 2145 Sheridan Road, Evanston, IL 60208, USA.

(email: lchen@anl.gov, l-chen@northwestern.edu and lupingyu@uchicago.edu)

Contents

Experimental Section

Unless stated specifically, all chemicals obtained from commercial suppliers were used without further purification. All solvents were purified with a standard distillation procedure prior to use. All reactions were carried out under nitrogen atmosphere. Monomers **2**,[1] **6**,[2] **8**[3] and **9**[4] were prepared according to previous literatures. ^{1}H NMR spectra were recorded on a Bruker DRX-400 spectrometer, with tetramethylsilane as an internal reference. Elemental analysis was performed by Midwest MicroLab. The number- and weight-average molecular weights of the polymers were determined by gel-permeation chromatography (GPC) with a Waters Associates liquid chromatography instrument equipped with a Waters 510 HPLC pump, a Waters 410 differential refractometer, and a Waters 486 tunable absorbance detector. Chloroform was used as the eluent and polystyrene as the standard. TGA measurement of the polymers was performed using a TA Q600 instrument under N_2 flow. UV−vis absorption spectra were measured on a Shimadzu UV-3600 device. Cyclic voltammetry was performed on an AUTOLAB/PG-STAT12 model system with a three-electrode cell in a 0.1 N Bu_4NBF_4 solution in acetonitrile at a scan rate of 100 mV/s. A film of each polymer was coated onto a Pt wire electrode by dipping the electrode into a polymer solution in chloroform. All measurements were calibrated against an internal standard of ferrocene (Fc), the ionization potential (IP) value of which is −4.8 eV for the Fc/Fc+ redox system. The contact angle measurements were performed using a KSV (Helsinki, Finland) CAM 200 contact angle goniometer. Dynamic light scattering was carried out on Malvern Zetasizer Nano, and the scattering angle of 173º was used. Cobalt content was determined by inductively coupled plasma mass spectrometry (ICP-MS), where the sample was first digested by H_2SO_4/H_2O_2 solvent at 90 ºC for 24 h.

Transient Absorption Spectroscopy: Femtosecond transient absorption spectra were performed on an apparatus based on a commercial Ti:sapphire laser system. A 1 kHz pulse train of ~100 fs, 2.9 mJ 830 nm pulses was generated by a Spitfire Pro regenerative (regen) amplifier (Spectra-Physics), which was seeded

by a Mai Tai oscillator also pumped by an Empower (Spectra-Physics). The regen output was used to generate the pump and probe beams. The 491 nm (PBDT-bpy) pump pulse was generated by a home-built, white-light seeded, dual-pass optical parametric amplifier (OPA).[5] Briefly, a small percentage of the regen output was focused into a sapphire disk to generate a white light continuum, which was mixed in the dual-pass OPA with a 415 nm beam generated by doubling the regen output in a BBO crystal. The probe beam was generated by focusing the remaining portion of the regen output into a sapphire crystal to form a white light continuum ranging from 450 to 780 nm. TA experiments were performed using a commercial Helios pump probe spectrometer (Ultrafast Systems LLC) using fiber optic/CCD detection. The sample was pumped with 491 or 550 nm, 100 nJ pulses chopped at 500 Hz. The instrument response function (IRF) for the pump-probe setup was ~300 fs. TA data were chirp corrected by analyzing the nonresonant $CHCl_3$ solvent response using the Surface Xplorer software (Ultrafast Systems LLC). Fits to the kinetics traces were also carried out using the Surface Xplorer software. Experiments were performed at room temperature in a 2 mm cuvette. The sample headspace was purged briefly with N_2 before measurements, and samples were constantly mixed for the duration of the experiment using a magnetic stir bar. Sample integrity was monitored using steady-state absorption spectroscopy.

Synthesis of Polymer

PBDT-bpy: A mixture of monomers **6** (0.084 g, 0.100 mmol), monomer **2** (0.0314 g, 0.100 mmol) and $Pd(PPh_3)_4$ (5.8 mg, 5 mol%) was weighed into a 15 mL round-bottom flask. Then 8 mL of anhydrous toluene and 2 mL of anhydrous dimethylformamide (DMF) were added under nitrogen. The mixture was degassed for 15 min and then heated at 120 °C for 24 h. After cooling to room temperature, the mixture was added to methanol. The precipitate was dissolved in chloroform, filtered with Celite and further stirred in saturated EDTA aqueous solution for 30 min to remove the metal catalyst. The polymer solution was dried with anhydrous Na_2SO_4, filtered, concentrated and precipitate into methanol. The polymer powder was

washed by Soxhlet extraction with methanol, hexane and chloroform. The final polymer was obtained after reprecipitation with methanol, yielding 55 mg (yield 83%). ^{1}H NMR (CDCl3): δ 3.2 −4.7 (30H, br), 7.30 −8.50 (8H, br). GPC: M_n (23.8 kg/mol), M_w/M_n (1.84). Elemental analysis: calcd for $C_{34}H_{40}N_2O_8S_2$: C, 61.06; H, 6.03; N, 4.19; O, 19.14; S, 9.59; found: C 58.50, H 5.70 N, 3.59; S, 9.50.

PPDI-bpy: A mixture of monomers **9** (0.100 g, 0.099 mmol), monomer **2** (0.0314 g, 0.100 mmol), Pd(*t*-$Bu_3P)_2$ (2.6 mg, 5 mol%) and Pd(PPh3)4 (5.8 mg, 5 mol%) was weighed into a 15 mL round-bottom flask. Then 8 mL of anhydrous toluene containing 1 drop of Aliquot 336 and 2 mL of K_2CO_3 aqueous solution (1.0 M) were added under nitrogen. The mixture was degassed for 15 min and then heated at 120 ℃ for 24 h. After cooling to room temperature, the mixture was added to methanol. The precipitate was dissolved in chloroform, filtered with Celite and further stirred in saturated EDTA aqueous solution for 30 min to remove the metal catalyst. The polymer solution was dried with anhydrous Na_2SO_4, filtered, concentrated and precipitate into methanol. The polymer powder was washed by Soxhlet extraction with methanol, hexane and chloroform. The final polymer was obtained after reprecipitation with methanol, yielding 50 mg (yield 53%). ^{1}H NMR (CDCl3): δ 0.6 −2.4 (52H, br), δ 5.1 −5.2 (2H, br), 7.30 −8.90 (12H, br). GPC: M_n (12.2 kg/mol), M_w/M_n (2.46). Elemental analysis: calcd for $C_{60}H_{68}N_4O_4$: C, 79.26; H, 7.54; N, 6.16; O, 7.04; found: C 77.20, H 7.87 N, 5.95.

Hydrogen Evolution Experiments: In order to carry out the photocatalytic reaction in DEA/water solution, 2 mg of the polymer was first dissolved in chloroform and titrated with a desired amount of $CoCl_2$ ethanol solution in a 6 mL vial. Drying of polymer solution under N_2 at constant flow rate for 20 min resulted in a transparent solid film, which was further suspended in a pre-degassed diethylamine/water mixture (2.0 mL, 3/7, v/v) and stirred vigorously in the dark for 24 h to furnish a uniform suspension. Then, the suspension was transferred into a home-made quartz cell (rectangular, 12mm×12mm×50mm), which was sealed with a gas-tight rubber cap. Nitrogen was bubbled for 2 min in the solution phase and 2 min in the gas

phase at a fixed flow rate inside the reactor to remove the residual oxygen. The quartz cell was put in the chamber of spectrophotometer (Fluorolog-3, Horiba), and the reaction mixture was illuminated with a 450 W Xe light-source. Circulating water was supplied to maintain the reaction temperature to be 25 °C. Gas samples were taken with a gas-tight syringe, and analyzed by GC. Hydrogen was detected with a thermal conductivity detector referencing against standard gas with a known concentration of hydrogen. Hydrogen dissolved in the diethylamine/water solution was not measured and the pressure increase generated by the evolved hydrogen was neglected in the calculations.

Apparent Quantum Yield (AQY) calculation: In the following we describe the **AQY** determination at $_0$ = 350 nm for PBDT-BPY. The energy (E) of irradiation was determined to be 60.0 mW by a calibrated power meter. The number of incident photons (N_0) is 7.9×10^{16} s^{-1} as calculated by equation (1), where T% represents the transmittance of the home-made quartz cell. The volume (V) of H_2 molecules generated in 9 h was determined to be 12.4 μL. The number of collected H_2 is 9.9×10^{12} s^{-1} as calculated by equation (2). The quantum efficiency is calculated from equation (3):

$$N_0=\frac{E\lambda T\%}{hc}=\frac{60\times10^{-3}\times350\times10^{-9}\times0.75}{6.63\times10^{-34}\times3\times10^{8}}\mathrm{s}^{-1}=7.9\times10^{16}\mathrm{s}^{-1} \quad (1)$$

$$N=\frac{V\times6.02\times10^{23}}{22.4t}=\frac{12.4\times10^{-6}\times6.02\times10^{23}}{22.4\times9\times3600}\mathrm{s}^{-1}=9.9\times10^{12}\mathrm{s}^{-1} \quad (2)$$

$$AQY=\frac{2N}{N_0}=2.5\times10^{-4} \quad (3)$$

Electronic Structure Calculations. All DFT calculations were carried out using Gaussian 09,[6] revision A.02, software installed on the Blues cluster at Argonne National Laboratory. For all calculations, the B3LYP[7-9] hybrid exchange-correlation functional was used in combination with a TZVP[10] basis set for all atoms. Spin-restricted and spin-unrestricted formalisms were used for all polymers, respectively. Time-dependent DFT (TD-DFT) single-point calculations were carried out on gas-phase optimized models

using the same combination of functional and basis set. Solvation effects ($CHCl_3$) were included using the polarized continuum model (PCM).[11] Wave function contours were generated using the β-LUMO[12] program and population analyses were carried out using the QMForge[13] program. Molecular models were built using GaussView 5.0.8 software.[14] The first coordination sphere of Co(II) was chosen as tetrahedral, high-spin (S = 3/2) $Co(bpy)Cl_2$; this is based on the absence of additional coordinating ligands in $CHCl_3$. Side-chains of the BDT portion were truncated with capping hydrogen atoms.

The geometric and electronic structures of polymer PBDT-bpy and Co(II) chelated polymer PBDT-bpy were investigated in more detail using DFT and TD-DFT methods. Two models of polymer PBDT-bpy were considered: 1) a monomer polymer PBDT-bpy model, which is a single D-A unit (BDT-bpy), and 2) a dimer polymer PBDT-bpy model, which is a two repeat D-A-D-A unit ($(BDT\text{-}bpy)_2$). Mulliken population analyses for the monomer and dimer models of polymer PBDT-bpy are given in Table S20 and S21, respectively, while a population analysis for the Co(II)-chelated monomer is given in Table S6. As discussed below, the major frontier molecular orbitals involved in the visible absorption spectrum of PBDT-BPY are the HOMO-1, HOMO, LUMO, and LUMO+2. Both the HOMO-1 and LUMO orbitals are delocalized over both the BDT-bpy unit due to conjugation, while the HOMO and LUMO are localized on the BDT and bpy units, respectively. The DFT derived energy level diagrams are given in Figure S4. Upon Co(II)-chelation to the monomer model of polymer PBDT-bpy, the unoccupied LUMO orbitals are strongly stabilized in energy due to an electrostatic stabilization upon binding the cationic transition metal (~1.0 eV). The HOMO energies are only minimally stabilized (~0.1 eV). This is given pictorially in Figure S20 (from left to right). Upon binding Co(II), the previously delocalized HOMO-1 and LUMO orbitals of polymer PBDT-BPY take on more localized character (HOMO-1: 68.8/31.2 → 85.0/14.8 and LUMO: 43.0/47.0 → 19.6/79.5). These changes are consistent with the energy level diagram obtained from electrochemistry.

The experimental UV-vis spectrum of polymer PBDT-bpy is given in Figure S21a. We tentatively assign

the absorption to two main electronic transitions (regions 1 and 2). Region 1 is located at ~500 nm (~20 000 cm^{-1}) and appears to have vibronic structure with an energy spacing between 0-0, 0-1, and 0-2 transitions of ~1500 cm^{-1}, which would correspond to symmetric in-plane vibrations of the polymer PBDT-bpy backbone. Region 2 is at ~400 nm (~25,000 cm^{-1}). The TD-DFT calculated UV-vis spectra for polymer PBDT-bpy monomer (red line) and dimer (green) models is given in Figure S21b and is overlaid with the experimental spectrum for comparison (black line). Note that transitions 1 and 2 are both calculated at higher energy in the monomer model but shift down in energy upon formation of the dimer. Again, monomer and dimer results are similar, however, and both agree well with the experimental data. For the monomer polymer PBDT-bpy, transitions 1 and 2 are predicted to be HOMO → LUMO and HOMO-1 → LUMO transitions and are thus intramolecular transitions of the polymer backbone. From population analyses, these correspond to more localized BDT → mixed BDT/bpy and mixed BDT/bpy → mixed BDT/bpy transitions, respectively. Upon Co(II) chelation (Figure S21b, blue line), both calculated transitions 1 and 2 are red-shifted in energy (black arrows), as observed experimentally (Figure 2a of the main text). They also pick up greater charge transfer character due to partial localization (*vide supra*), but are dominantly intramolecular transitions of the polymer backbone. We note that higher energy transitions of the PBDT-bpy model (e.g., state 3 in Table S7) show greater charge transfer character than states 1 and 2. Interestingly, the calculated oscillator strengths go as 2 > 1 > 3, which is similar to the overlap of the donor and acceptor orbitals involved in the transitions (2 > 1 > 3). The decreased overlap, however, reflects more localized donor (BDT) and acceptor (bpy) based orbitals, however (see Table S4). Thus, it follows that the charge transfer character is 3 > 1 > 2. Higher charge transfer character for higher-energy excited states may play an important role in the QY of PBDT-bpy. Lastly, DFT calculations on a PPDI-bpy model show that both the HOMO and LUMO levels are fully localized on PDI (Figure S22), in agreement with UV-vis and electrochemistry.

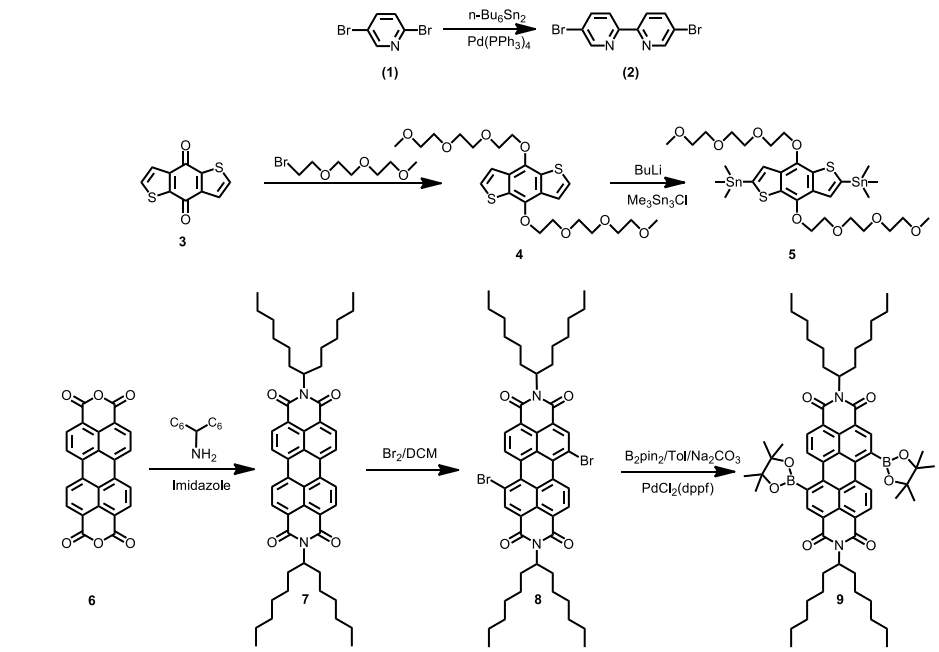

Scheme S1. Schematic of synthetic routes to the synthesized monomers.

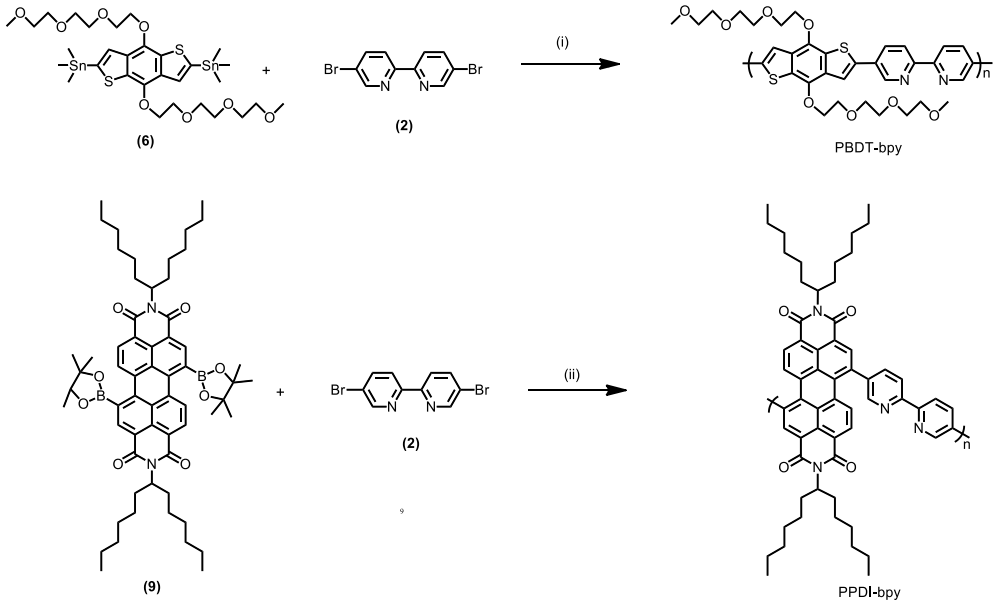

Scheme S2 Schematic of synthesis of polymers. (i) $Pd(PPh_3)_4$, Toluene/DMF, 24 h; (ii) $Pd(t\text{-}Bu_3P)_2$, $Pd(PPh_3)_4$, Toluene/K_2CO_3, 24 h.

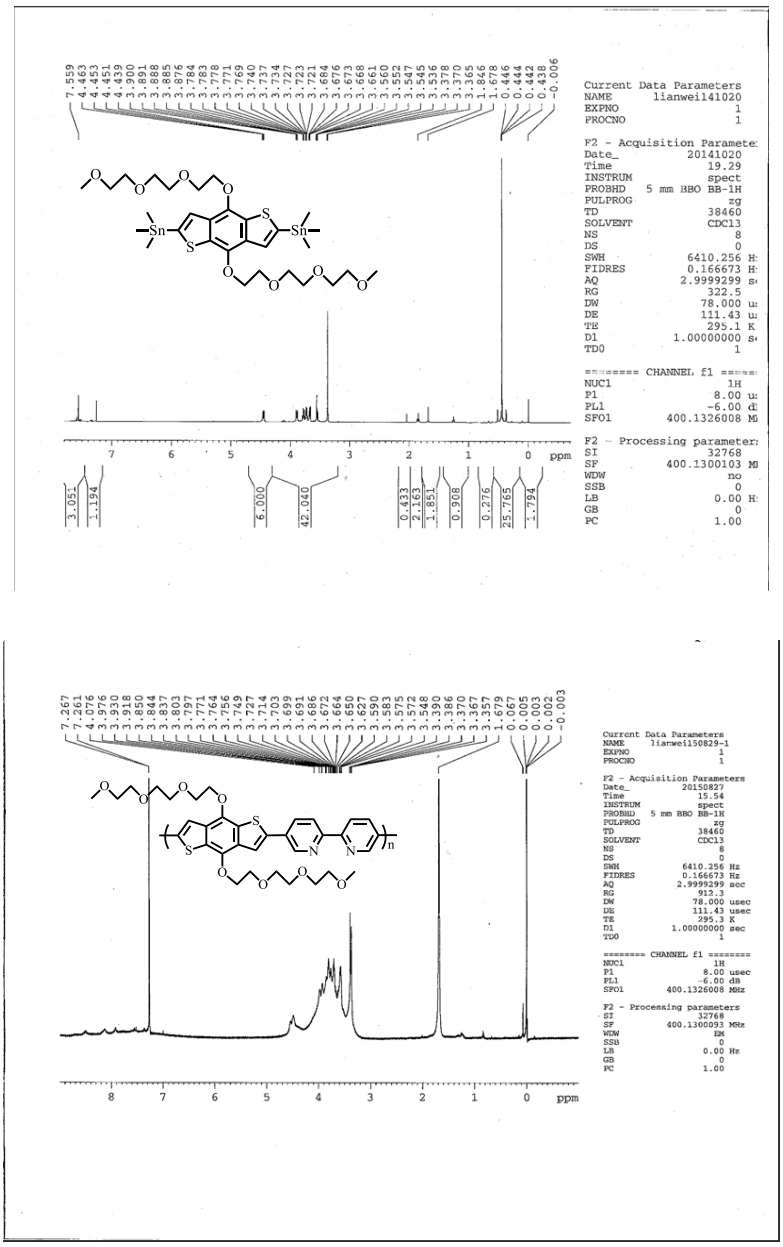

Figure S1. ^{1}H-NMR spectra of polymer PBDT-bpy and its monomer precursor.

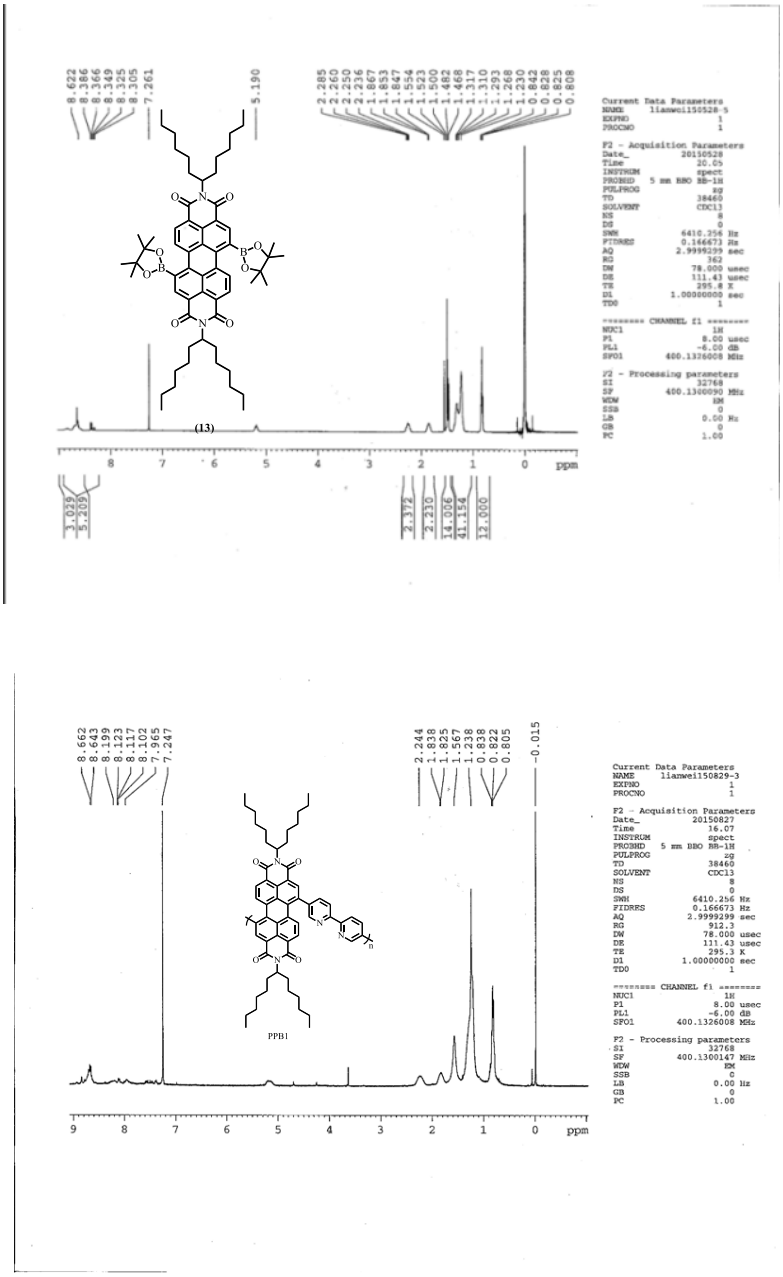

Figure S2. [1]H-NMR spectra of polymer PPDI-bpy and its monomer precursor.

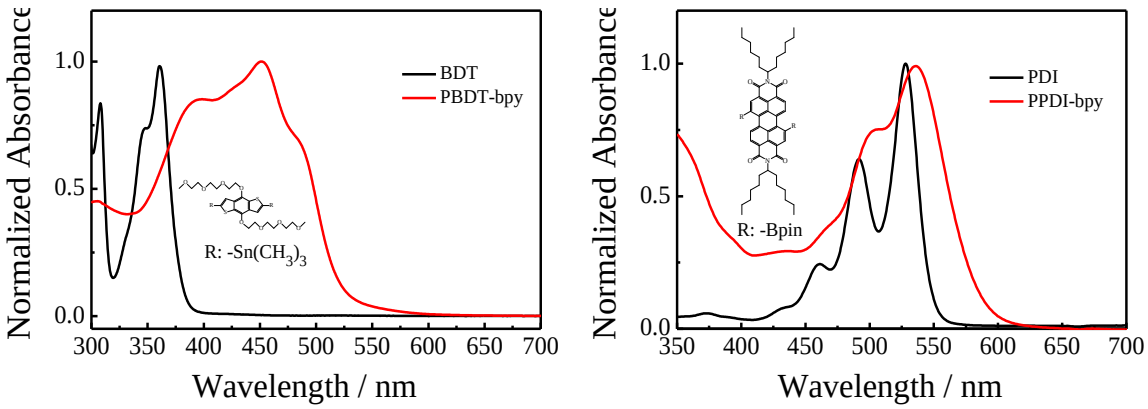

Figure S3. UV−vis absorption spectra of the prepared polymers and their monomer precursors in chloroform.

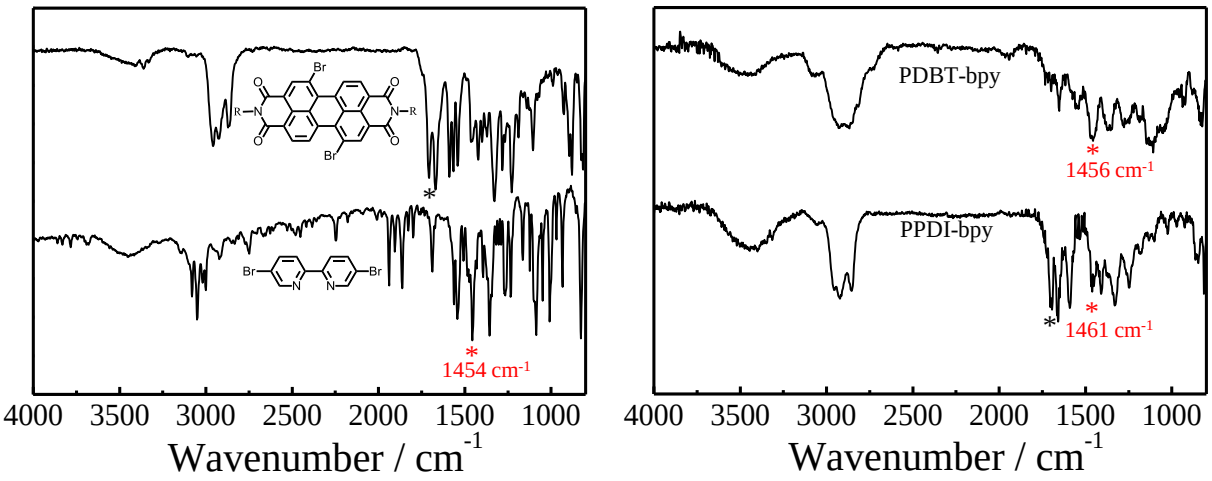

Figure S4. FTIR spectra of the prepared polymers and their monomer precursors.

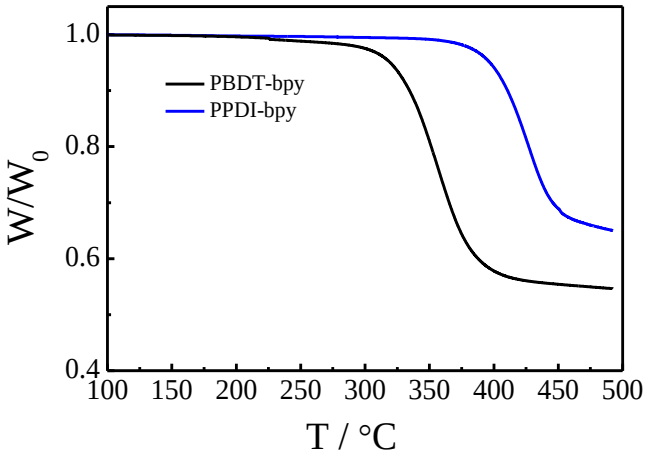

Figure S5. TGA spectra of the two polymers.

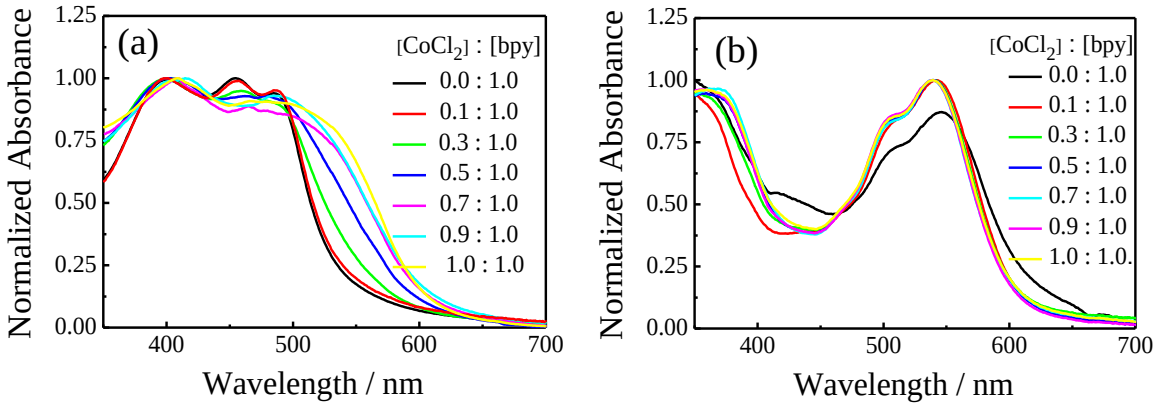

Figure S6. (a) UV−vis absorption spectra of polymer PBDT-bpy titrated with $CoCl_2$ in films gained from drop-casting onto clean glass. (b) UV−vis absorption spectra of polymer PDPI-bpy titrated with $CoCl_2$ in films gained from drop-casting onto clean glass.

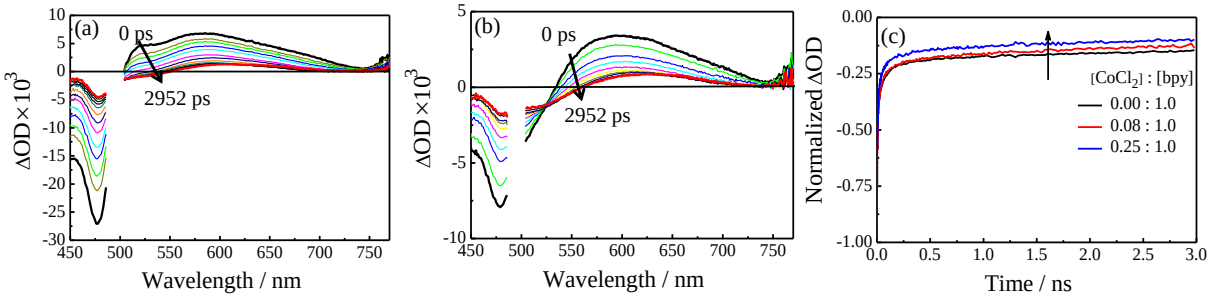

Figure S7. Transient absorption spectra of polymer PBDT-bpy (491 nm excitation) titrated with 0% (**a**) and 25% (**b**) Co(II) ($CoCl_2$ in EtOH). (**c**), Kinetics of the ground state recovery measured at 477 nm (arrow indicates accelerated ground state recovery upon Co(II) titration). Spectra in (**a**) and (**b**) are at: 0.5 (black line), 0.7, 1, 2, 5, 10, 25, 50, 100, 202, 502, 1002, 2002, 2952 (red line) ps.

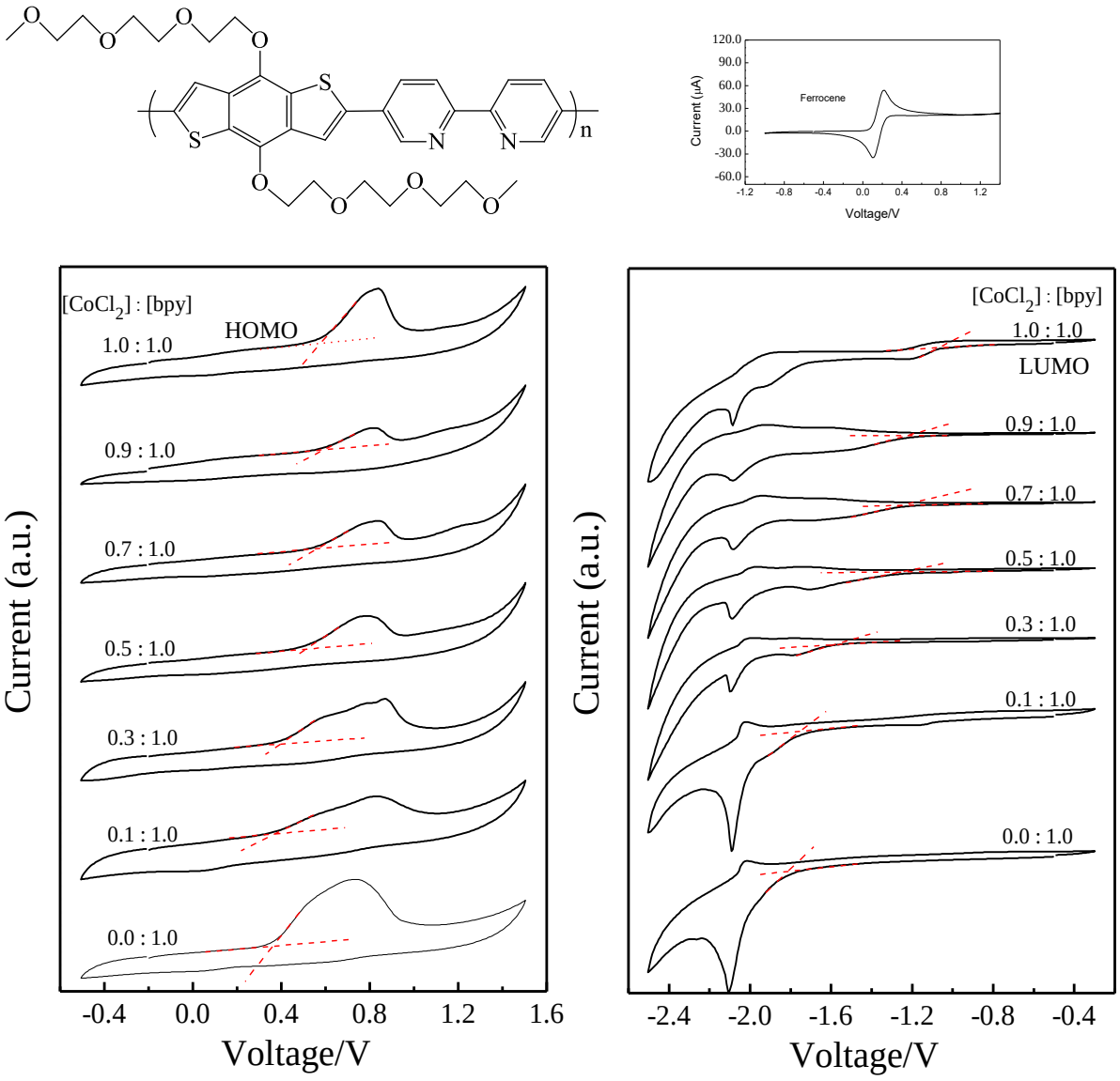

Figure S8. Cyclic voltammetry results for polymer PBDT-BPY films.

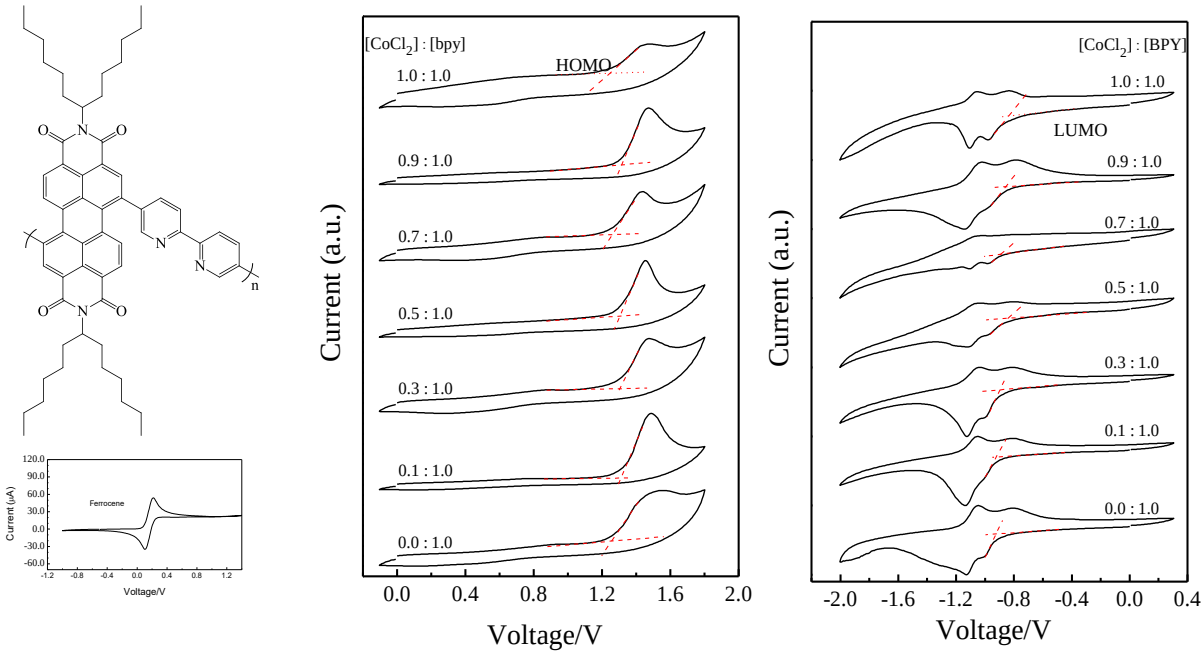

Figure S9. Cyclic voltammetry results for polymer PPDI-BPY films.

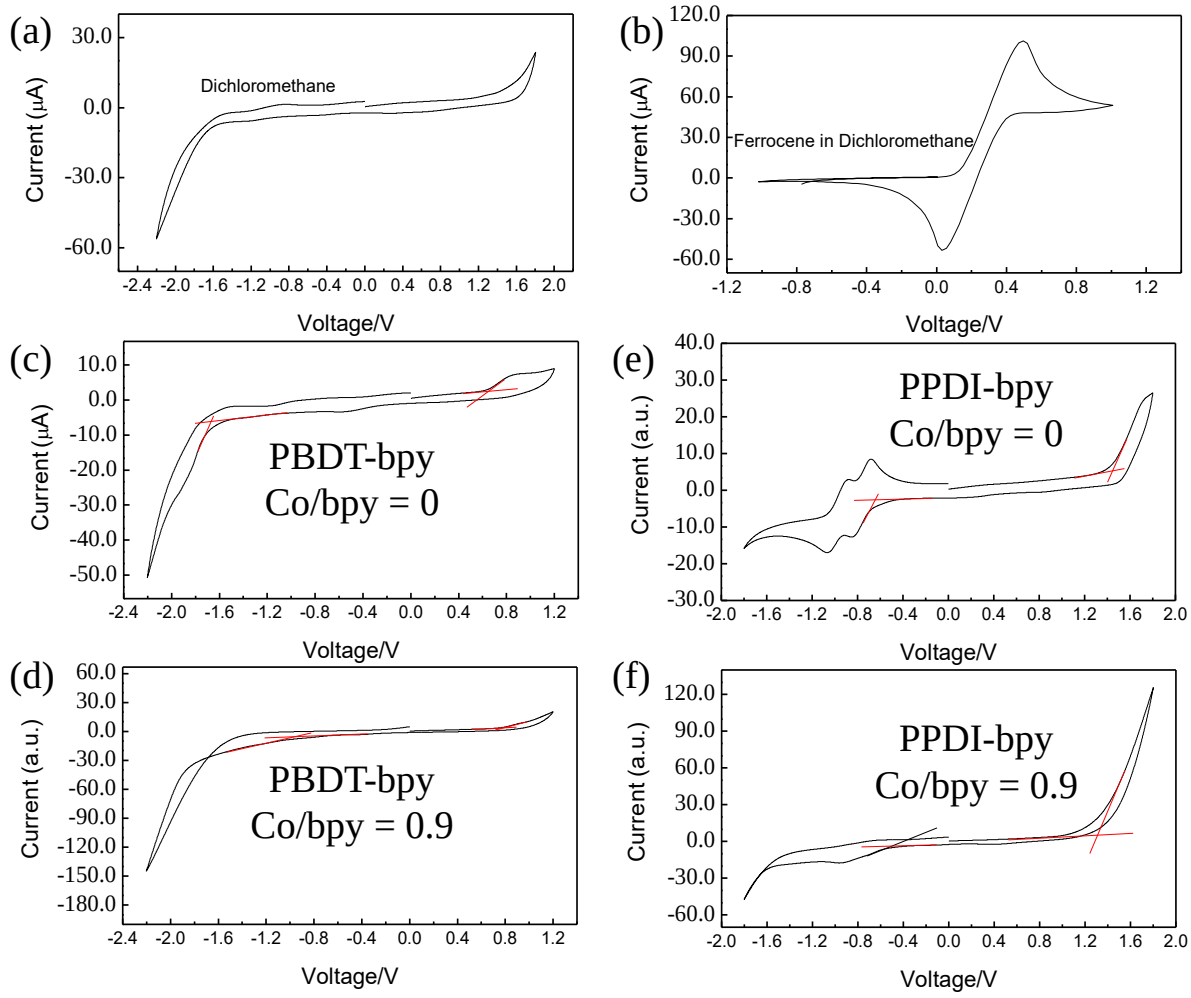

Figure S10. Cyclic voltammetry results for polymers PBDT-bpy and PPDI-BPY in dichloromethane.

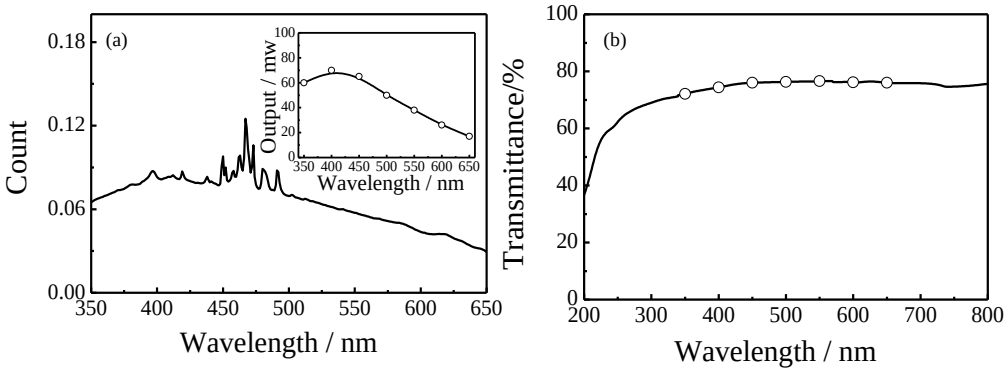

Figure S11. (a) Output profiles of the 450 W Xe-bulb and output intensity of each individual mono wavelength used in this study. (b) Wavelength dependence of transmittance of the homemade quartz cell.

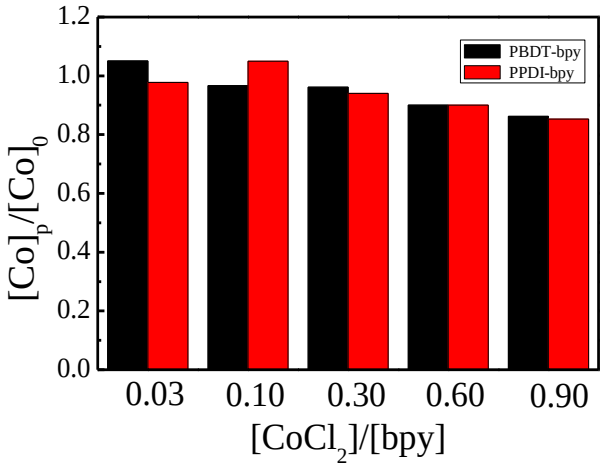

Figure S12. ICP-MS results for polymer solid after photocatalytic reaction, where the $[Co]_0$ and $[Co]_p$ represent the cobalt content loaded on the polymer solid before and after the photocatalytic reaction.

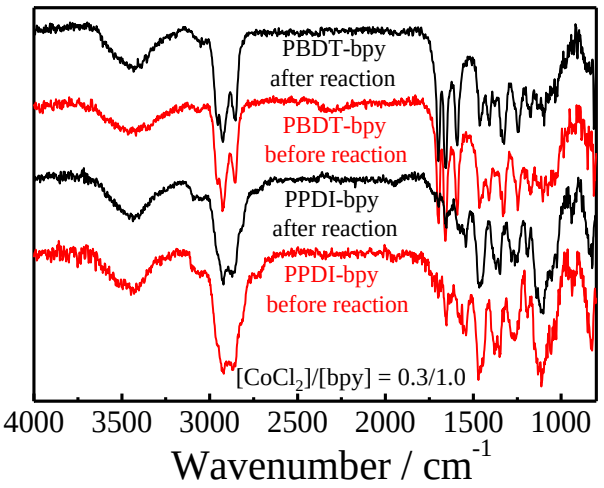

Figure S13. FTIR spectra of PBDT-bpy and PPDI-bpy before and after photocatalytic reaction.

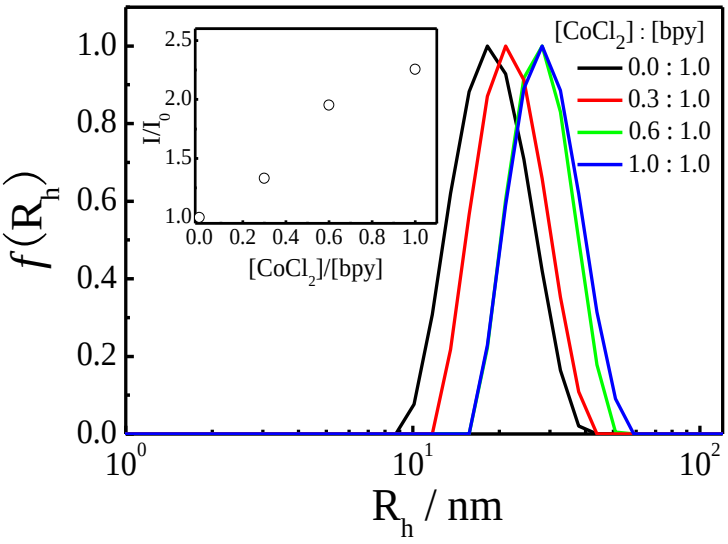

Figure S14. Hydrodynamic distributions of PBDT-bpy titrated with different contents of $CoCl_2$ in chloroform, where the inset Figure shows how the relative scattered intensity varies with the cobalt content.

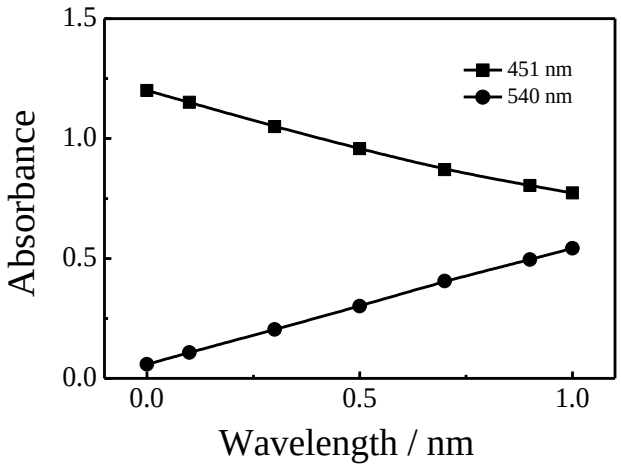

Figure S15. The optical densities at two characteristic wavelengths as a function of the cobalt ion concentration for PBDT-bpy in chloroform.

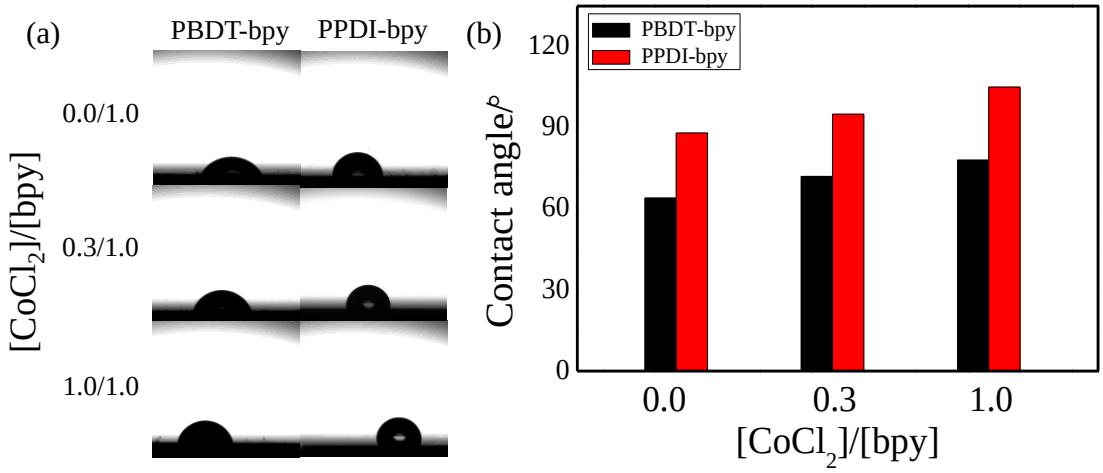

Figure S16. Contact angle measurement results for polymers with different cobalt contents, where the polymer chloroform solutions were drop-casted onto silicon wafer and air-dried before the measurements.

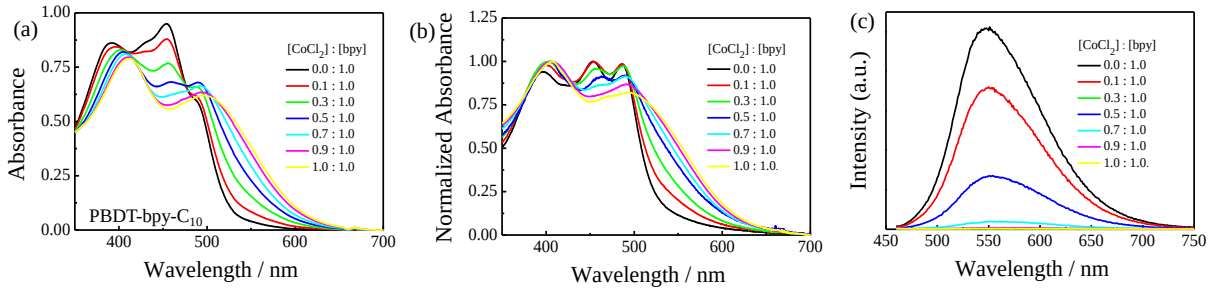

Figure S17. (**a**), UV−vis absorption spectra of PBDT-bpy-C_{10} titrated with $CoCl_2$ (in EtOH) in chloroform. (**b**), Film UV−vis absorption spectra of PBDT-bpy-C_{10} titrated with $CoCl_2$ (in EtOH) (generated by drop-casting onto clean glass). (**c**), Fluorescence spectra (450 nm excitation) of PBDT-bpy-C_{10} titrated with $CoCl_2$ (in EtOH) in chloroform solution.

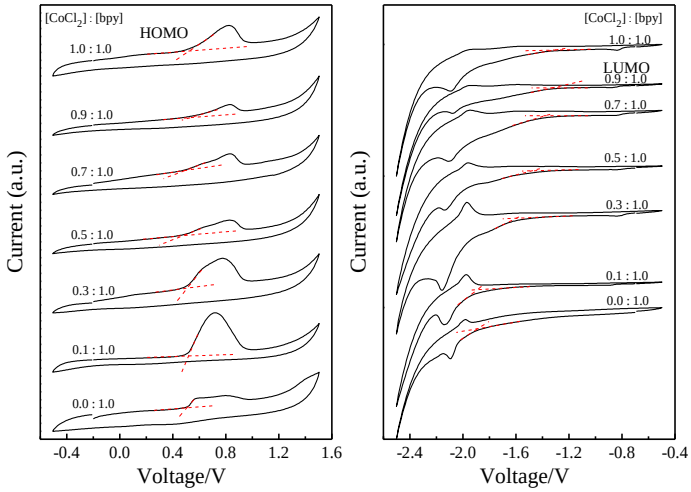

Figure S18. Cyclic voltammetry results for polymer PBDT-bpy-C_{10}.

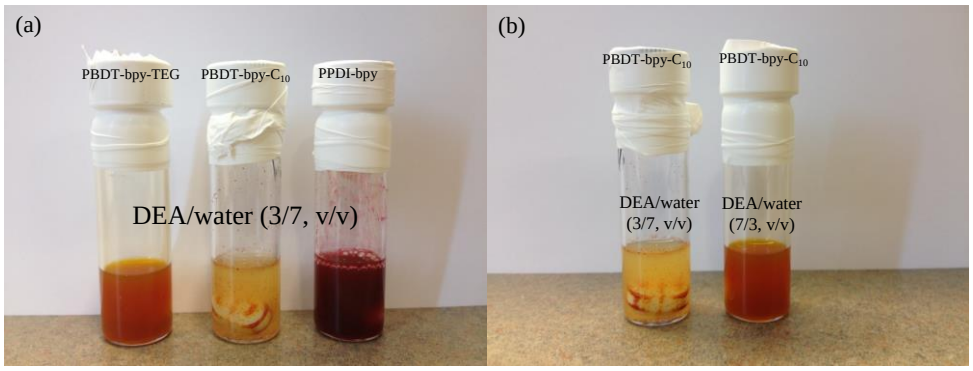

Figure S19. Photographs of polymers suspending in different solvent conditions.

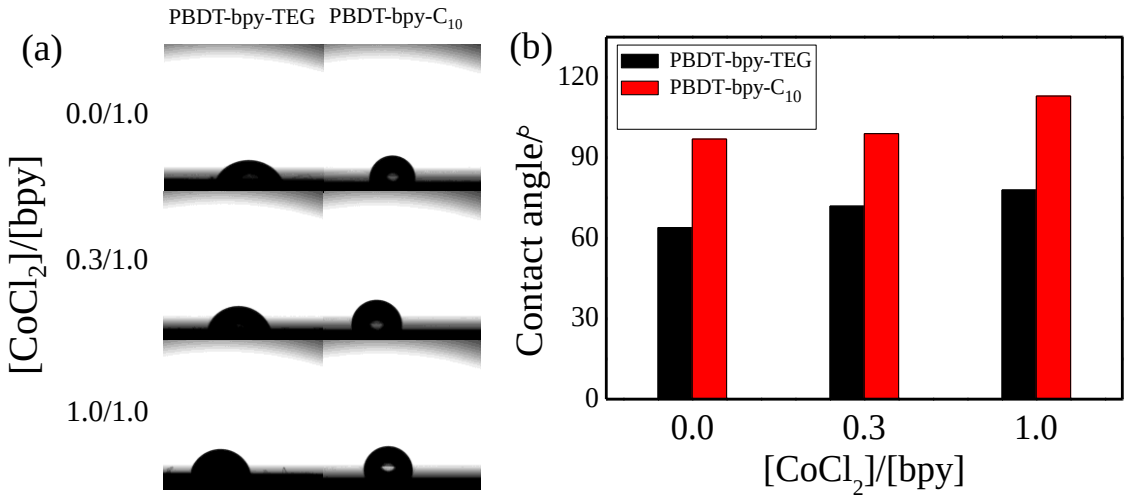

Figure S20. Contact angle measurement results for PBDT-bpy-TEG and PBDT-bpy-C_{10} with different cobalt contents, where the polymer chloroform solutions were drop-casted onto silicon wafer and air-dried before the measurements.

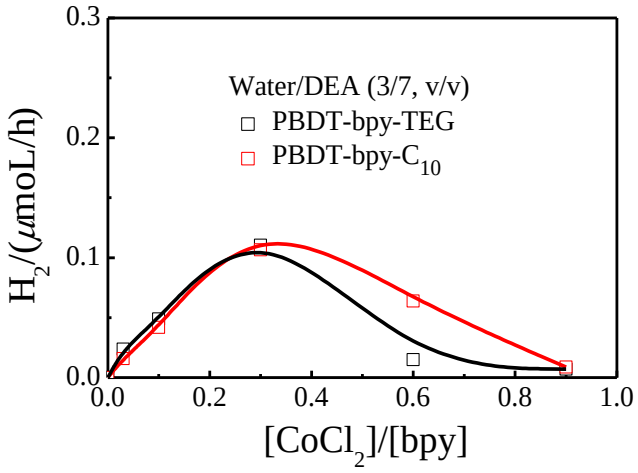

Figure S21. [$CoCl_2$]/[bpy] dependence of photocatalytic hydrogen production rates of PBDT-bpy-TEG and PBDT-bpy-C_{10} with different cobalt contents from water.

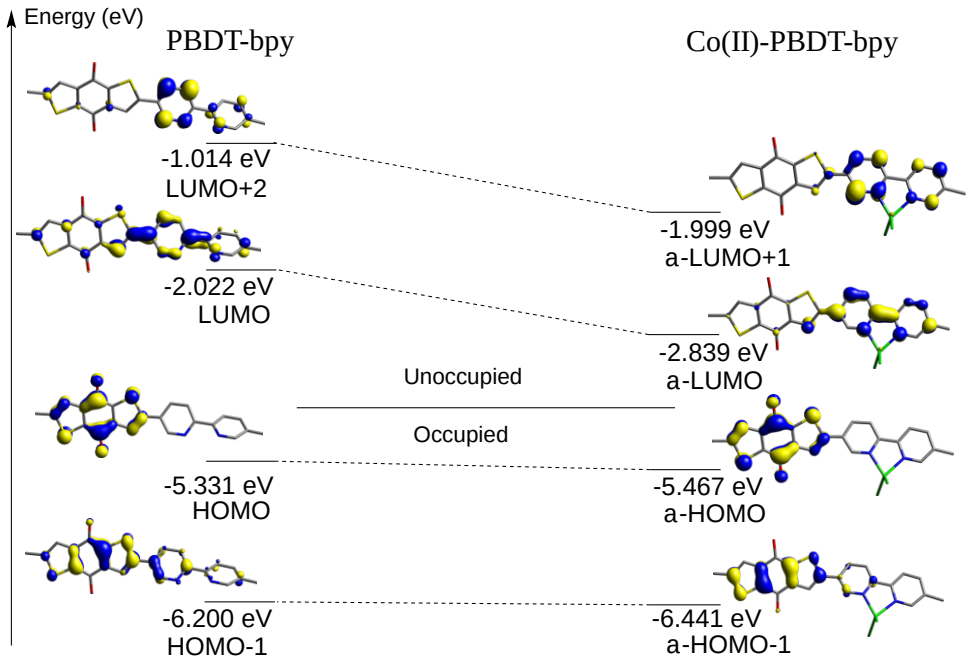

Figure S22. Molecular orbital diagram for the monomer model polymer PBDT-bpy and Co(II)-chelated PBDT-bpy. Note that only the α-spin MOs are shown on the right.

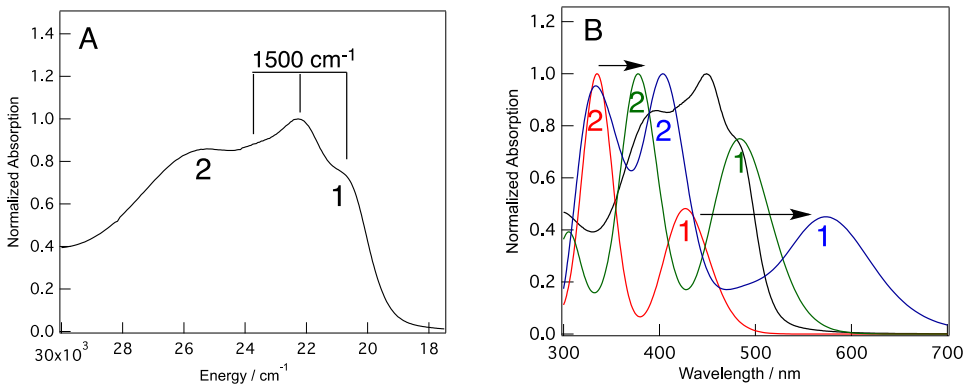

Figure S23. Comparisons between experimental and TD-DFT simulated absorption spectra. (A) Room temperature absorption spectrum of polymer PBDT-bpy in $CHCl_3$. (B) Black: polymer PBDT-bpy (exp.), Red: monomer polymer PBDT-bpy model; Green: dimer polymer PBDT-bpy model; Blue: Co(II)-chelated monomer polymer PBDT-bpy model.

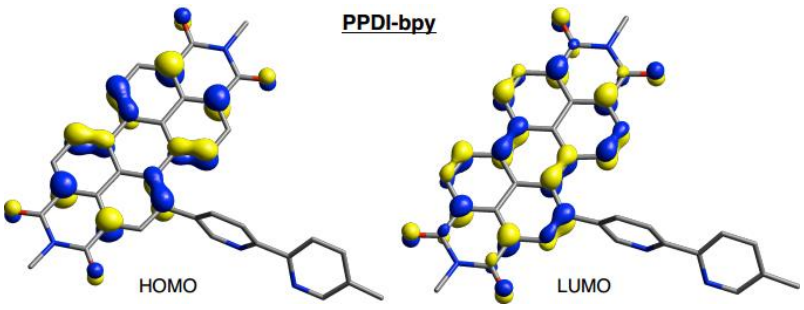

Figure S24. Molecular orbital diagram for the monomer model polymer PPDI-bpy

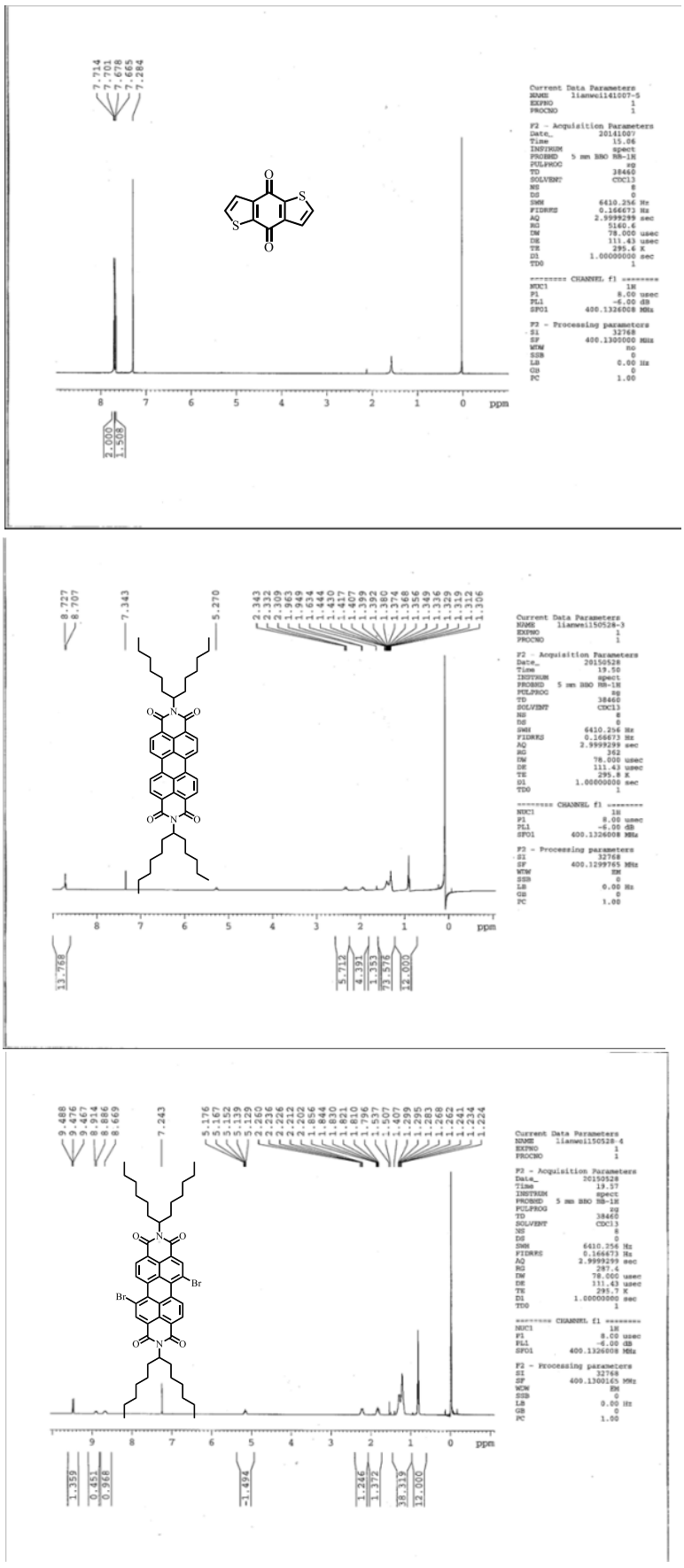

Figure S25. ^{1}H-NMR spectra of the intermediate compounds in $CDCl_3$.

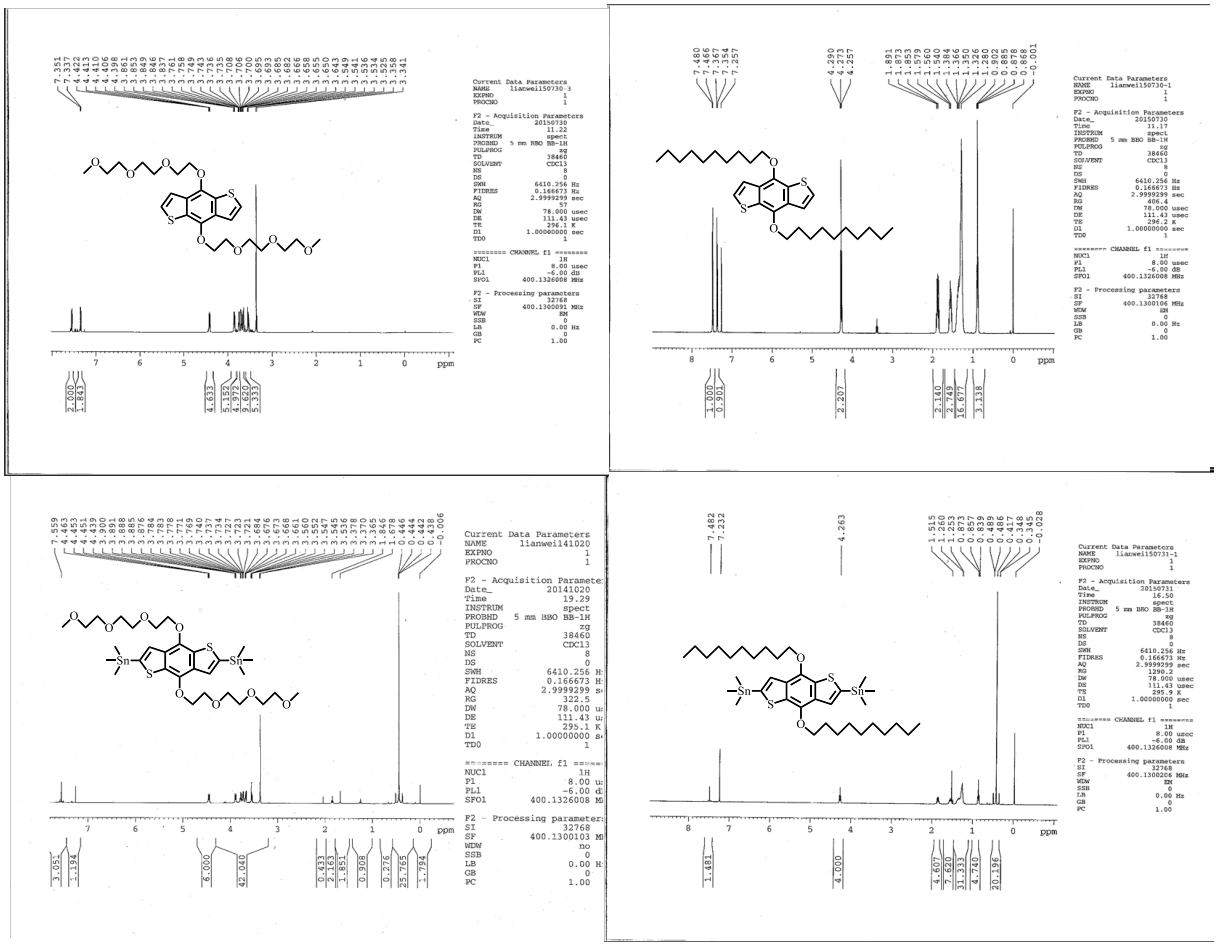

Figure S26. ^{1}H-NMR spectra of the intermediate compounds in $CDCl_3$.

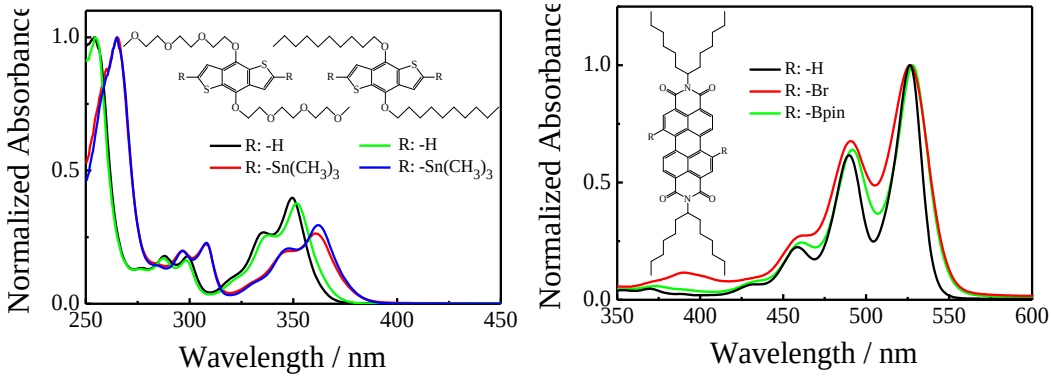

Figure S27. UV−vis absorption spectra of the monomers in $CHCl_3$.

Table S1. Element analysis results for the two polymers.

	Theory				Found			
Polymer	**C**	**H**	**N**	**S**	**C**	**H**	**N**	**S**
PBDT-bpy	61.07	6.03	4.19	9.59	58.50	5.70	3.59	9.50
PPDI-bpy	79.26	7.54	6.16	--	77.20	7.87	5.95	--

Table S2. Kinetic fits to the ground state bleach features in the transient absorption data.[a]

	0% Co(II)	8% Co(II)	25% Co(II)
A_∞[b]	-5 x 10^{-3} (15 %)[c]	-2.5 x 10^{-3} (12 %)	-1.9 x 10^{-3} (10 %)
A_1	-16. 2x 10^{-3} (47 %)	-10.2 x 10^{-3} (49 %)	-9.4 x 10^{-3} (49 %)
τ_1	0.8 ± 0.04	1.0 ± 0.05	0.9 ± 0.05
A_2	-8.8 x 10^{-3} (26 %)	-5.7 x 10^{-3} (27 %)	-5.4 x 10^{-3} (28 %)
τ_2	15.2 ± 1	18.1 ±1	12.0 ± 1
A_3	-4.3 x 10^{-3} (12 %)	-2.4 x 10^{-3} (12 %)	-2.4 x 10^{-3} (13 %)
τ_3	253 ± 23	450 ± 46	247 ± 23

[a] 477nm probe. Three exponential functions were used for the fits.

[b] Constant offset step function used in the fits.

[c] Percentage weight of the exponential function in the fits.

Table S3. Kinetic fits to the excited state absorption features in the transient absorption data.[a]

	0% Co(II)	8% Co(II)	25% Co(II)
A_∞[b]	1.2 x 10^{-3} (16 %)[c]	0.6 x 10^{-3} (12 %)	0.59 x 10^{-3} (9 %)
A_1	2.18 x 10^{-3} (29 %)	1.81 x 10^{-3} (36 %)	2.56 x 10^{-3} (40 %)
τ_1	1.2 ± 0.1	1.8 ± 0.4	1.4 ± 0.1
A_2	2.75 x 10^{-3} (37 %)	1.88 x 10^{-3} (37 %)	2.34 x 10^{-3} (37 %)
τ_2	15.7 ± 1	23.0 ± 1	16.6 ± 1
A_3	1.33 x 10^{-3} (18%)	0.76 x 10^{-3} (15 %)	0.9 x 10^{-3} (14 %)
τ_3	186 ± 24	586 ± 58	365 ± 33

[a] 585 nm probe. Three exponential functions were used for the fits.

[b] Constant offset step function used in the fits.

[c] Percentage weight of the exponential function in the fits.

Table S4. Experimental feeding ratios for PBDT-bpy and PPDI-bpy before CV or UV-vis measurement.

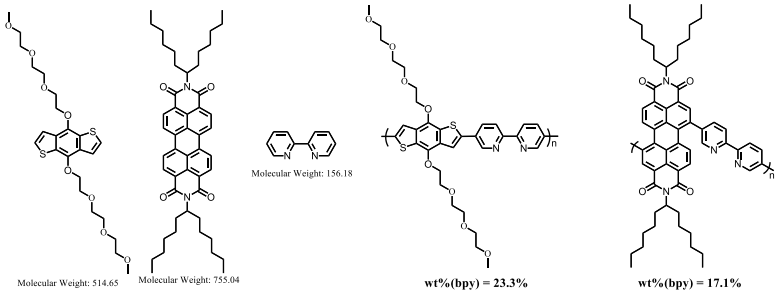

Entry	PBDT-bpy (3.0 mg/mL)	$CoCl_2$ (5.76 mg/mL)	Co/bpy ratio	Entry	PPDI-bpy (3.0 mg/mL)	$CoCl_2$ (5.76 mg/mL)	Co/bpy ratio
1	0.5 mL	0 μL	0	1	0.5 mL	0 μL	0
2	0.5 mL	5 μL	0.1	2	0.5 mL	3.7 μL	0.1
3	0.5 mL	15 μL	0.3	3	0.5 mL	11.0 μL	0.3
4	0.5 mL	25 μL	0.5	4	0.5 mL	18.4 μL	0.5
5	0.5 mL	35 μL	0.7	5	0.5 mL	25.7 μL	0.7
6	0.5 mL	45 μL	0.9	6	0.5 mL	33.0 μL	0.9
7	0.5 mL	50 μL	1.0	7	0.5 mL	36.7 μL	1.0

Table S5 Cobalt content-dependent hydrogen production rate of polymer photocatalysts

DEA/H_2O (3/7, v/v)			
PBDT-bpy		PPDI-bpy	
$[CoCl_2]$/[bpy]	H_2/(μmol/h)	$[CoCl_2]$/[bpy]	H_2/(μmol/h)
0	0.011	0	0.006
0.03	0.047	0.01	0.025
0.06	0.10	0.03	0.11
0.1	0.28	0.1	0.16
0.2	0.23	0.3	0.57
0.3	0.037	0.6	0.71
0.6	0.011	0.9	0.011
0.9	0.005		

Table S6 Cobalt content-dependent hydrogen production rate of PBDT-bpy-TEG and PBDT-bpy-C_{10}.

DEA/H_2O (7/3, v/v)			
PBDT-bpy-TEG		PBDT-bpy-C_{10}	
$[CoCl_2]$/[bpy]	H_2/(μmol/h)	$[CoCl_2]$/[bpy]	H_2/(μmol/h)
0	0.008	0	0.007
0.03	0.024	0.03	0.0158
0.1	0.049	0.1	0.042
0.3	0.11	0.3	0.11
0.6	0.015	0.6	0.064
0.9	0.007	0.9	0.009

Table S7. Polymer PBDT-bpy (BDT-bpy) monomer Mulliken population analysis.[a]

	Energy (eV)	BDT	bpy
H-1(104)	-6.200	68.80	31.20
H(105)	-5.331	95.41	4.59
L(106)	-2.022	43.02	56.98
L+2(108)	-1.014	16.32	83.68

[a] Polarized continuum model with $CHCl_3$ as a solvent. HOMO-LUMO gap: 3.310 eV.

Table S8. Polymer PBDT-bpy $(BDT\text{-}bpy)_2$ dimer Mulliken population analysis.[a]

	Energy (eV)	BDT(1)	bpy(1)	BDT(2)	bpy(2)	BDT(t)[b]	bpy(t)[b]
H-8	-7.303	2.03	4.41	6.44	87.12	8.47	91.53
H-3	-6.329	26.96	20.18	43.30	9.66	70.26	29.84
H-2	-6.172	41.17	9.65	28.70	20.47	69.87	30.12
H-1	-5.418	74.22	3.93	18.95	2.90	93.17	6.83
H	-5.346	16.75	1.02	77.00	5.23	93.75	6.35
L	-2.425	32.77	10.47	11.11	45.65	43.88	56.12
L+1	-1.984	21.93	39.90	19.81	20.36	41.74	60.26
L+2	-1.513	19.37	26.22	33.58	20.83	52.95	47.05
L+6	-0.976	6.99	81.64	5.56	5.81	12.55	87.45

[a] Polarized continuum model with $CHCl_3$ as a solvent. HOMO-LUMO gap: 2.921 eV.

[b] Total BDT and bpy character for the dimer.

Table S9. Polymer PBDT-bpy -Co(II) (BDT-bpy) monomer Mulliken population analysis.[a]

α-spin	Energy (eV)	BDT	bpy	Co	Cl
H-1(136)	-6.441	85.01	14.81	0.09	0.09
H(137)	-5.467	96.23	3.75	0.01	0.01
L(138)	-2.839	19.64	79.50	0.47	0.39
L+1(139)	-1.999	14.49	84.63	0.61	0.27
β-spin					
H-2(132)	-6.490	32.08	3.91	33.95	30.06
H-1(133)	-6.414	53.32	12.14	19.27	15.26
H(134)	-5.466	96.18	3.80	0.01	0.01
L(135)	-3.029	10.24	71.38	16.00	2.38

[a] Polarized continuum model with $CHCl_3$ as the solvent. α(HOMO-LUMO) gap: 2.682 eV; β(HOMO-LUMO) gap: 2.438 eV.

Table S10. Time-dependent DFT results for the polymer PBDT-bpy monomer.[a]

State	E/nm	E/cm^{-1} (x 10^3)	E/eV	*f*[b]	Assignment
1	426.9	23.4	2.90	0.5336	H → L (0.70)
2	337.5	29.6	3.67	0.9453	H-1 → L (0.69)
3	332.5	30.1	3.73	0.0125	H → L+1 (0.62)
4	320.9	31.2	3.86	0.2780	H → L+2 (0.59)
5	301.6	33.2	4.11	0.0189	H → L+3 (0.66)

[a] All calculated states with energies < 300 nm. Polarized continuum model with $CHCl_3$ as the solvent. States considered here are bolded.

[b] Calculated oscillator strengths.

Table S11. Time-dependent DFT results for the polymer PBDT-bpy dimer.[a]

State	E/nm	E/cm^{-1} (x 10^3)	E/eV	f[b]	Assignment
1	483.5	20.7	2.56	1.4025	H → L (0.62)
2	465.4	21.5	2.66	0.0081	H-1 → L (0.62)
3	405.7	24.7	3.06	0.0422	H → L+1 (0.49) ; H-1 → L+1 (-0.49)
4	394.8	25.3	3.14	0.2168	H-1 → L+1 (0.49); H → L+1 (0.47)
5	376.6	26.6	3.29	1.6943	H-2 → L (0.68)
6	352.4	28.4	3.52	0.0043	H → L+2 (0.48); H-3 → L (-0.42)
7	348.6	28.7	3.56	0.0091	H-3 → L (0.50); H → L+2 (0.36)
8	345.6	28.9	3.59	0.1407	H-1 → L+2 (0.59)
9	338.7	29.5	3.66	0.0160	H → L+3 (0.47); H-1 → L+3 (-0.44)
10	334.8	29.9	3.70	0.0283	H → L+5 (0.44); H-1 → L+3 (0.40)
11	326.2	30.7	3.80	0.0102	H-1 → L+4 (0.56)
12	323.6	30.9	3.83	0.0197	H-2 → L+1 (0.64)
13	319.7	31.3	3.88	0.0021	H → L+5 (0.47); H → L+3 (-0.38)
14	310.6	32.2	3.99	0.0131	H-1 → L+5 (0.49)
15	310.3	32.2	4.00	0.0124	H-4 → L (0.52)
16	308.7	32.4	4.02	0.1237	H-3 → L+1 (0.40)
17	306.7	32.6	4.04	0.1948	H-8 → L (0.51)
18	305.1	32.8	4.06	0.2906	H → L+6 (0.35)
19	303.0	33.0	4.09	0.0057	H-1 → L+6 (0.45)

[a] All calculated states with energies < 300 nm. Polarized continuum model with $CHCl_3$ as the solvent. States considered here are bolded.

[b] Calculated oscillator strengths.

Table S12. Time-dependent DFT results for the polymer PBDT-bpy -Co(II) monomer.[a]

State	E/nm	E/cm^{-1} (x 10^3)	E/eV	*f*[b]	Assignment
1	2302.2	4.3	0.54	0.0000	BH-3 → L+1 (0.48); BH-3 → L (0.48); BH-3 → L+4 (-0.46)
2	1925.4	5.2	0.64	0.0000	BH-2 → L+2 (0.71); BH-1 → L+1 (0.55); BH-11 → L+2 (0.42)
3	1666.5	6.0	0.74	0.0002	BH-2 → L (0.392); BH-2 → L+2 (0.38); BH-2 → L+4 (-0.33)
4	960.7	10.4	1.29	0.0009	BH-3 → L+6 (0.83); BH-10 → L+6 (0.36)
5	796.8	12.6	1.56	0.0014	BH-3 → L+2 (0.90); BH-10 → L+2 (0.37)
6	692.0	14.5	1.79	0.0033	BH → L (0.69); AH → L (-0.56)
7	676.4	14.8	1.83	0.0030	BH-2 → L+6 (0.63); BH-1 → L+6 (0.49); BH-11 → L+6 (0.35)
8	575.3	17.4	2.16	0.2504	AH → L (0.69); BH → L (0.69)
9	490.3	20.4	2.53	0.0838	BH → L+1 (0.78); AH → L (-0.40)
10	476.4	21.0	2.60	0.0046	BH-1 → L (0.59); AH-1 → L (0.51)
11	427.2	23.4	2.90	0.0440	AH → L+1 (0.70); BH → L+1 (0.49)
12	418.2	23.9	2.96	0.0013	BH-2 → L (0.69); BH-1 → L (0.39)
13	406.9	24.6	3.05	0.2357	BH-1 → L (0.47); AH-1 → L (-0.35); AH → L+1 (0.34)
14	401.7	24.9	3.09	0.2908	AH-1 → L (0.59); BH-2 → L (0.37); AH → L+1 (0.36)
15	384.1	26.0	3.23	0.0012	BH-3 → L (0.84); BH-3 → L+1 (-0.38)
16	380.5	26.3	3.26	0.0104	BH-4 → L (0.40); BH → L+3 (0.30)
17	375.4	26.6	3.30	0.0003	BH → L+2 (0.99)
18	366.5	27.3	3.38	0.0218	BH → L+3 (0.62); BH-1 → L+1 (-0.31)
19	361.9	27.6	3.43	0.0898	BH → L+3 (0.52); BH-1 → L+1 (0.40); AH → L+2 (-0.31)
20	359.1	27.8	3.45	0.0016	AH-2 → L (0.97)
21	358.3	27.9	3.46	0.0014	AH-3 → L (0.66); AH-6 → L (-0.56); AH-5 → L (-0.34)
22	354.4	28.2	3.50	0.1526	AH → L+2 (0.72); BH → L+3 (0.35)

[a] All calculated states with energies < 300 nm. Polarized continuum model with $CHCl_3$ as the solvent. States considered here are bolded.

[b] Calculated oscillator strengths.

Supplementary References.

1. Schwab PFH; Fleischer F; Michl J *J. Org.*Chem. **2002**, *67*, 443.

2. Lu K; Fang J; Zhu X; Yan H; Li D; Di Ca; Yang Y; Wei Z *New J Chem.* **2013**, *37*, 1728.

3. Dubey RK; Efimov A; Lemmetyinen H *Chem. Mater.* **2011**, *23*, 778.

4. Dey S; Efimov A; Lemmetyinen H *European J. Org.*Chem. **2011**, *76*, 5955.

5. Greenfield, S. R. & Wasielewski, M. R. Near-transform-limited visible and near-IR femtosecond pulses from optical parametric amplification using Type II β-barium borate. *Opt. Lett.* **1995**, *20*, 1394.

6. Frisch, M. J.; Trucks, G. W.; Schlegel, H. B.; Scuseria, G. E.; Robb, M. A.; Cheeseman, J. R.; Scalmani, G.; Barone, V.; Mennucci, B.; Petersson, G. A.; Nakatsuji, H.; Caricato, M.; Li, X.; Hratchian, H. P.; Izmaylov, A. F.; Bloino, J.; Zheng, G.; Sonnenberg, J. L.; Hada, M.; Ehara, M.; Toyota, K.; Fukuda, R.; Hasegawa, J.; Ishida, M.; Nakajima, T.; Honda, Y.; Kitao, O.; Nakai, H.; Vreven, T.; Montgomery, J. A., Jr.; Peralta, J. E.; Ogliaro, F.; Bearpark, M.; Heyd, J. J.; Brothers, E.; Kudin, K. N.; Staroverov, V. N.; Keith, T.; Kobayashi, R.; Normand, J.; Raghavachari, K.; Rendell, A.; Burant, J. C.; Iyengar, S. S.; Tomasi, J.; Cossi, M.; Rega, N.; Millam, J. M.; Klene, M.; Knox, J. E.; Cross, J. B.; Bakken, V.; Adamo, C.; Jaramillo, J.; Gomperts, R.; Stratmann, R. E.; Yazyev, O.; Austin, A. J.; Cammi, R.; Pomelli, C.; Ochterski, J. W.; Martin, R. L.; Morokuma, K.; Zakrzewski, V. G.; Voth, G. A.; Salvador, P.; Dannenberg, J. J.; Dapprich, S.; Daniels, A. D.; Farkas, O.; Foresman, J. B.; Ortiz, J. V.; Cioslowski, J.; Fox, D. J. *Gaussian 09*, revision D.01; Gaussian, Inc.: Wallingford, CT, 2009.

7. Stephens, P. J.; Devlin, F.J.; Chabalowski, C. F.; Frisch, M. J. *J. Phys. Chem.* **1994**, *98*, 5648.

8. Lee, C.; Yang, W.; Parr, R. G. *Phys. Rev. B.: Condens. Matter Mater. Phys.* **1998**, *37*, 785.

9. Becke, A. D. *J. Chem. Phys.* **1993**, *98*, 5648.

10. Schaefer, A.; Huber, C.; Ahlrichs, R. *J. Chem. Phys.* **1994**, *100*, 5829.

11. Miertus, S.; Scrocco, E.; Tomasi, J. *Chem. Phys.* **1981**, *55*, 117.

12. Kieber-Emmons, M. T. *Lumo*, version 0.9b; Burlingame, CA. 2011.

13. Tenderholt, Adam L. *QMForge*, Version 2.4, http://qmforge.sourceforge.net.

14. GaussView, Version 5, Dennington, R.; Keith, T.; Millam, J. *Semichem Inc.*, Shawnee Mission, KS, 2009.